Alpine glacier surface velocity measurement from UAV imagery – examining the effect of image resolution on the accuracy of results

Neamat Karimi

GEOCARTO INTERNATIONAL
https://doi.org/10.1080/10106049.2022.2043454

Alpine glacier surface velocity measurement from UAV imagery – examining the effect of image resolution on the accuracy of results

Neamat Karimi

Department of Water Resources Research, Water Research Institute, Tehran, Iran

ABSTRACT

The reliability and validity of the Glacier Surface Velocity (GSV) measurement results based on remote sensing datasets depends on the quality and spatial resolution of the image used. The typical pixel size of space-borne satellite imagery is often larger than the annual and inter-annual displacement of small alpine debris-covered glaciers. In addition, the pixel size of medium resolution satellite images (10–30 m), limits the size of a feature that can be matched. This is even more of an issue for glaciers located in arid and semi-arid environments (e.g. glaciers in Iran and high mountains of Asia) where flow velocities are not exceeding a few metres per year. Consequently, high-resolution data such as Unmanned Aerial Vehicle (UAV) images are required to calculate the surface velocity of such glaciers. However, the optimal resolution of UAV images is one of the most important challenges in GSV measurement. This paper explores the influence of UAV image resolution on the quality of GSV results. Analysis was carried out at 19 different resolutions of UAV images from 10 to 100 cm with a 5 cm bin over a debris-covered glacier, in Iran. COSI-Corr algorithm was used to perform the image correlation. To evaluate the accuracy of obtained results, manual digitisation was performed and the differences between manual GSV and frequency cross-correlator were assessed for all data sets. Moreover, displacement calculated for a stagnant off-glacier area was evaluated. While the quality of the results of the images between 10 and 30 cm is substantially the same, the obtained results indicate that the best result of GSV was not obtained using the finest image resolution. Results revealed that the highest correspondence between the measured GSV and manual digitisation was obtained in a 30 cm spatial resolution image. In addition, the 30 cm image resolution shows the minimum uncertainty over the off-glacier static area. Obtained results revealed that using too fine resolution images will lead to computational redundancy, while no improvement is observed in the accuracy of GSV results.

ARTICLE HISTORY
Received 29 July 2021
Accepted 12 February 2022

KEYWORDS
Glacier surface velocity; image resolution; UAV; debris-covered glaciers; COSI-Corr; manual digitisation

CONTACT Neamat Karimi n.karimi@wri.ac.ir

1. Introduction

Since the turn on the twenty-first century, glaciers around the world are getting thinner (Dehecq et al. 2019; Gentili et al. 2020). The shrinking and disappearing of glaciers in recent decades have remarkable impacts in terms of natural hazards (e.g. ice avalanches, glacier break-offs and glacial lake outburst floods), sea-level rise, food security, and increasing restrictions on freshwater resources (Kääb et al. 2018; Millan et al. 2019; Rai et al. 2019). Hence, as targeted through the International Panel for Climate Change (IPCC) (Intergovernmental Panel on Climate Change 2014), tracking glacier and ice sheet change have turned out to be a first-rate assignment of the twenty-first century.

Due to the relatively rapid and proportionate responses of glaciers to any adjustments in weather variables, tracking any glacier geometry change is consequently of key importance to apprehend how climate changes affect the status of glaciers (Gentili et al. 2020). Also, to increase the ability to predict the future status of glaciers in the coming decades, it is essential to study the dynamics of glaciers in more details (Tanarro et al. 2019). In addition, several models used for estimating the ice thickness distribution of mountain glaciers depend strongly on the quality of input data (Millan et al. 2019). One of the most important indicators of glacier dynamics is the glacier flow which transfers ice and the deposited debris covers from accumulation areas to the low elevation ablation parts (Lo Vecchio et al. 2018). The velocity of this transformation is greatly depending on various factors such as glacier surface slope, ice thickness, and climatic fluctuations (Shukla and Garg 2020).

Glacier Surface Velocity (GSV) is determined by the reactivity of a glacier to climate change. Recent works have shown that the movement of mountain glaciers in response to climate change declined remarkably (Kraaijenbrink et al. 2016). For example, glaciers in Pamir slowed by 43% between 2000 and 2010 (Heid and Kääb 2012b), GSV in Nepal declined by 70% between 1982 and 2009 (Sugiyama et al. 2013). It is consequently crucial to improve tools and techniques to set up the present state and quantify ongoing changes of glaciers.

Taking into account the unaffordable nature of glaciers and due to the large area and inaccessibility of glaciated areas, any ground measurement (e.g. Global Positioning System, GPS, measurements and any other similar approaches) in these areas are very difficult and even impossible (Karimi et al. 2014; Paul et al., 2015). This difficulty is exacerbated in studies that should be conducted at different time intervals to examine the trend and dynamics of glaciers. Accordingly, remote sensing data has become an effective and powerful tool for study the glaciers and their dynamics (Farajzadeh and Karimi 2014).

Before the advent of Unmanned Aerial Vehicles (UAVs), nearly all information about the glacier velocities relies on terrestrial photogrammetry and global repeated coverage of the space-borne optical satellite images. Terrestrial (ground-based or close-range) photogrammetry is based on the estimation of glacier motion using a time-lapsed sequence of digital images from a fixed camera site overlooking the glacier (Maas et al. 2006; Ahn and Box 2010; Kaufmann 2012). The present approach is one of the first successful methods for glacier and rock glacier surface velocity measurement and has been used frequently in different kinds of debris-covered (Kaufmann and Ladstädter 2008), and debris-free glaciers (Evans 2000; Maas et al. 2006).

Space-borne approaches, mainly includes medium resolution Landsat, ASTER, and SPOT images. These often medium resolution images (10–30 m image resolution) hampered our knowledge on small alpine glaciers in mountain regions that have an area smaller than a few square kilometres (Dehecq et al. 2015, 2019; Millan et al. 2019; Ramsankaran et al. 2021). The spatial resolution of these satellite images is adequate for large-scale analysis and it is too coarse for GSV measurement at local scales, where the GSV may only be a few metres (Evans 2000). Therefore, it would be advantageous to use new technologies such as UAVs with the ease of digital and automated image processing to calculate GSV at high precision. UAV platforms have the vast capability to enhance the low resolution space-borne images by providing high-resolution images with exceedingly low costs in comparison to the spaceborne satellite images (e.g. GeoEye, Wordview, Pleiades, and, etc.) and airborne photos (Ramsankaran et al. 2021; Karimi et al. 2021b). Since 2010, UAV photogrammetry has been used frequently on alpine glaciers for elevation change analysis (Wigmore and Mark 2017; Bash et al. 2018; Jouvet et al. 2019), GSV measurement (Jouvet et al. 2018; Vivero and Lambiel 2019; Fey and Krainer 2020; Storni et al. 2020; Robson et al. 2021; Śledź et al. 2021), and mapping of glacier surface features (Fugazza et al. 2015; Kraaijenbrink et al. 2016). In recent years, the application of UAV surveys in high mountain glaciated Asia (especially in Himalaya) is gaining momentum for GSV and glacier dynamic monitoring (Immerzeel et al. 2014; Vincent et al. 2016), mapping glacier surface temperature (Kraaijenbrink et al. 2018) and glacier mass balance measurement (Brun et al. 2018; Watson et al. 2020). However, UAV studies in Asia's glaciers remain scarce. Because in comparison to the Alps or Andes, the terrain of most glaciers in Asia are hostile, highly debris-covered, and located in high altitudes. These factors make logistic much more difficult for UAV surveys in such glaciated areas. Using UAV data, we now have the ability to address two important questions (Vivero and Lambiel 2019; Fey and Krainer 2020): (1) obtain arbitrary spatial resolution images of small glacierized regions; and (2) have a temporal frequency of acquisition to monitoring the horizontal and vertical changes in the glacier on interannual to decadal.

The accuracy of GSV measurement from the UAV imageries largely depends on the status of the glaciers (e.g. the ratio of debris-covered areas to clean ice regions, the size of boulders and the degree of homogeneity of glacier surface), methodology used, the time intervals between UAV campaigns, the quality of image co-registration and the quality of the acquired images. In addition, the quality of images depends to a large extent on the spatial resolution of images or the Ground Sampling Distance (GSD). One of the main operational challenges in glaciology studies is the optimal flight height of UAVs (Ramsankaran et al. 2021) and it is associated obtained image resolutions to achieve a better GSV quality without excessively increasing flight time or processing.

Studies based on repeated images from the glacier (using space-borne satellite images or UAV imageries) have so far mostly focussed on obtaining the best results testing different image matching methods (e.g. Heid and Kääb 2012b; Redpath et al. 2013). However, no studies have concentrated on examining the effect of image resolution on GSV results. This is especially important when it comes to UAVs. It is therefore a need to examine the impact of image resolution over a locally representative small debris-covered glacier in order to assess an optimal image resolution for accurate and widely applicable measurement of GSV from repeated optical UAV data. The main goal of this study is therefore to look into different spatial resolution UAV images on image matching methods. Here we use 10–100 cm UAV images for quantitative evaluation of changes in image resolution on the accuracy of the GSV results. In this regard, two high-resolution UAV images (acquired in 2018 and 2020) from the largest debris-covered glacier in Iran were used. To evaluate the image resolution variation on GSV results, the COSI-Corr module, developed by (Leprince et al. 2007) was used.

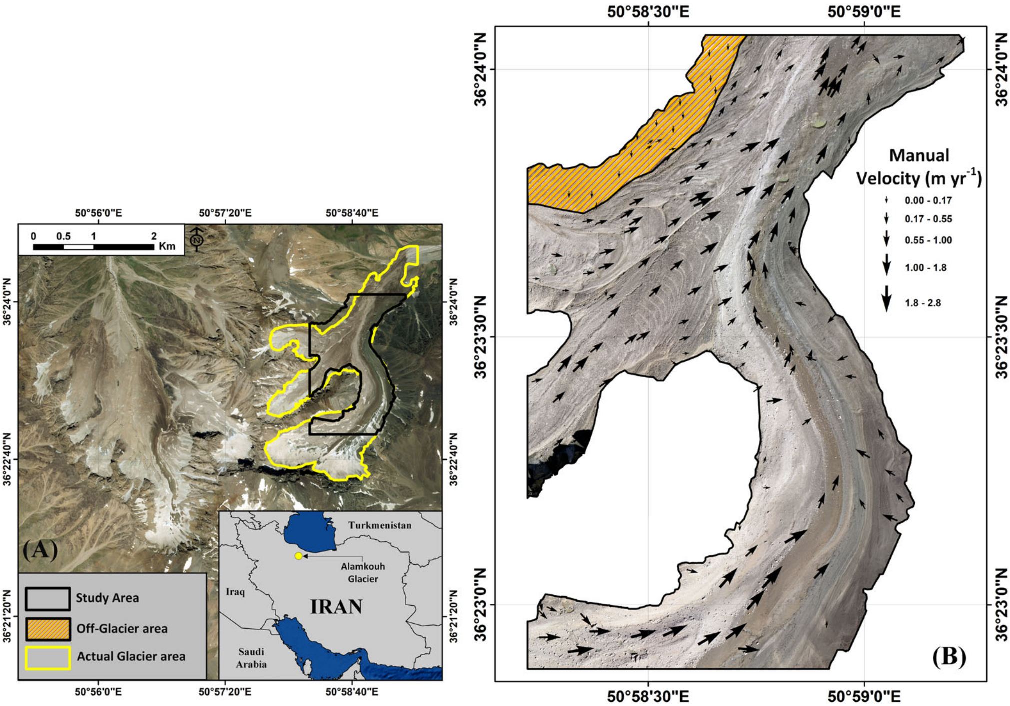

Figure 1. (A) Location map of the Alamkouh glacier. Yellow and black lines indicate the actual area of the Alamkouh glacier and the area of UAV image acquisition, respectively. (B) Overview of the study area and the location of manual digitisation points. The location of the off-glacier stable area was shown with orange hash.

2. Study area

In order to evaluate the effect of UAV image resolution on GSV results, the debris-covered Alamkouh glacier in Iran was selected. Recent studies revealed that most part of the Alamkouh glacier (about 88%) is debris covered (Karimi et al. 2014). This glacier spreads out from the maximum elevation of 4393 m above sea level (a.s.l) to about 3750 m a.s.l at the glacier tongue. Recent studies using LiDAR and UAV data revealed that Alamkouh glacier has been thinning at a rate of -0.23 ± 0.03 m yr^{-1} between 2010 and 2020 (Karimi et al. 2021a, 2021b). In addition, using multi-temporal satellite and UAV images over the last 15 years (between 2005 and 2020) indicate that the mean annual GSV of Alamkouh glacier has not remain constant and variate in different periods without a clear increasing or decreasing trend (Karimi et al. 2022)

In the present study, the entire surface of the glacier area has not been studied and only the middle section of the glacier which includes the debris-covered areas along with the off-glacier stagnant area was selected to achieve the intended goals. The actual glacier area and the selected study area are shown in Figure 1 in yellow and black lines, respectively. Also, in order to accuracy assessment of the obtained GSV results, an off-glacier non-dynamic area was selected near the glacier. This stable area is shown as an orange hash in Figure 1(B).

3. Data and methods

3.1. UAV data acquisition

For GSV measurement and analysing the impact of image resolution on the accuracy of results, two UAV high-resolution images were used. These images were primarily used in other studies for elevation change analysis and mass balance measurements (Karimi et al. 2021a, 2021b). UAV acquisition campaigns were performed on study area at the end of ablation seasons (September) of 2018 and 2020. These surveys were conducted using a small cost-effective and easy maintenance (in comparison to the fixed-wing systems) Phantom 4 PRO V2.0 system with 20MP onboard camera. Phantom 4 PRO V2.0 system can fly for about 15 to a maximum of 20 min in high elevation glaciated areas. By considering the flight altitude of 200 metres and 80% forward and side overlaps, mosaic images at approximately 0.25 km^2 can take in each flight. These UAV data acquisitions were described in Karimi et al. (2021a) in more detail.

3.2. UAV data processing

In order to generate ortho-images, aerial photos collected from both UAV surveys were processed using Pix4Dmapper software (https://www.pix4d.com) using high-quality settings. This software used structure from Motion (SfM) algorithm for DEM and ortho-image generation (Fey and Krainer 2020). Unlike classic photogrammetry, SfM uses computer vision algorithms to recognise matching characteristics in a set of overlapping aerial images, calculating the orientation and location of the camera. To obtain geographically accurate mosaic images, Ground Control Points (GCPs) are necessary. Totally, 93 and 121 GCPs were measured in 2018 and 2020 surveys respectively using Trimble R8 GPS over the glacier surface and off-glaciers areas. All GCPs were measured on detectable boulders over the glacier surface and off-glacier areas. These GCPs were collected initially for DEM generation by two different teams and as they are not collected on similar boulders and positions, they cannot be used for GSV measurement and accuracy assessment of COSI-Corr results. By marking all GCPs on the initial UAV images, georeferencing of the ortho-photos are obtained. The mean horizontal RMSE error of both 2018 and 2020 generated ortho-images are equal to 0.087 and 0.056 m, respectively.

As a result, an original 10 cm ortho-images were generated. The area covered by the original ortho-images from the case study area is about 3.89 km^2 but in the present study a debris-free area was removed and a subset of 1.8 km^2 was used. Both high-resolution UAV ortho-mosaic images were co-registered using 58 tie points over the off-glacier stable areas. The output ortho-images were resampled at 5 cm intervals and 19 orthophotos were generated with resolutions between 10 and 100 cm. The spatial resolutions considered for analysis are 10, 15, 20, 25, 30, 35, 40, 45, 50, 55, 60, 65, 70, 75, 80, 85, 90, 95 and 100 cm.

3.3. GSV measurement and accuracy assessment

In the present study, we adopted the COSI-Corr algorithm for image correlation (Leprince et al. 2007). Any horizontal ground displacement can be retrieved by COSI-Corr from the sub-pixel correlation of two different images. In COSI-Corr, image correlation is calculated with an iterative, unbiased processor that calculates the phase plane in the Fourier domain (Leprince et al. 2007; Scherler et al. 2008). This process leads to generates displacements in longitude (GSV_Y) and latitude (GSV_X) directions and the final displacement map was calculated as follows:

$$\text{Diss} = \sqrt{GSV_X^2 + GSV_Y^2}$$

Before applying COSI-Corr, all possible window sizes to identify the best and most accurate window sizes are evaluated. In this stage, we evaluate the performance of 32, 64, 128, 256, and 512 window sizes over 20, 30, 55, 75, and 90 cm images, by comparison, the outputs of COSI-Corr algorithms with manual digitisation points. After initial evaluating the obtained results, we found that several morphological changes occur over the glacier surface between two different UAV surveys (e.g. ice thinning, rolling boulders, formation of supraglacial lakes, and ice cliffs). Such unwanted features and disturbances have a negative impact on the final GSV results. To meet this challenge, a multi-scale frequency correlator mode was used in this study, because it has the potential to discard such noises (Leprince et al. 2007; Kraaijenbrink et al. 2016). In the multi-scale mode, first, the initial and final window sizes are preconfigured. Secondly, the displacement calculates from the larger initial window size to the smaller final size iteratively and if the correlation succeeds, it is re-executed with smaller window size and accounting for the displacement found in the previous stage. The process is iterated until the minimum window size is reached, or until the correlation fails. If the process fails, the displacement from the previous larger window size is kept. Therefore, the output of this part of the study will help to find the best initial window size to extract the most accurate GSV maps, while also savings processing time.

Considering that the main purpose of this study is to compare the accuracy of UAV images with different scales on estimating the GSV, the least possible post-processing was applied to the obtained results. The GSV results were post-processed using filters to discard the pixels with a signal-to-noise-ratio (SNR) value lower than 0.90 and then any aberrations related to the shadows, seasonal snow covers, and rapid ice melting around ice melting were removed from the GSV maps. At the end, relating the displacement to the period duration enabled the average annual GSV (m yr^{-1}).

We compared the results of all UAV images with resolutions from 10 to 100 cm based on their accuracy in measuring the magnitude of GSV. Two strategies were adopted for analysing the effect of the UAV image resolution on the accuracy of GSV measurement over the debris-covered glaciers. In the first strategy, manual digitisation was performed in GIS. In this step, about 110 visually detectable boulders over the study area were selected and their displacement was determined by comparing 2018 and 2020 UAV images. The location of all manual digitisation points over the glacier and off-glacier surfaces is shown in Figure 1(B).

Uncertainty of manual digitisation was assessed by multiple digitisation (5 GIS expert analysts) of pre-determined boulders. The results of the digitisation exercise of the GSV by five analysts show that the mean standard deviation of the GSV is about 3%. The highest differences in the GSV were found in large rotated boulders with a mean standard deviation of 5%. While in the small boulders the mean standard deviations is minimum. In addition, the recognizability of boulders is also an important parameter. Because in a limited number of cases where the contrast of the UAV images was low or the boulders were shaded, the standard deviation was higher.

Finally, to quantify the velocity differences in the final GSV maps, Root Mean Square Error (RMSE), and coefficient of determination (R^2) were measured between manual digitisation and the final COSI-Corr velocity results.

In the second strategy, displacement calculated by the COSI-Corr for a static off-glacier area was evaluated. As no surface displacement is expected in non-glaciated stable areas, any displacement is considered as the systematic biases (e.g. an error of co-registration) and the variance of the results indicates the measurement precision (as per Scherler and Strecker 2012; Karimi et al. 2022).

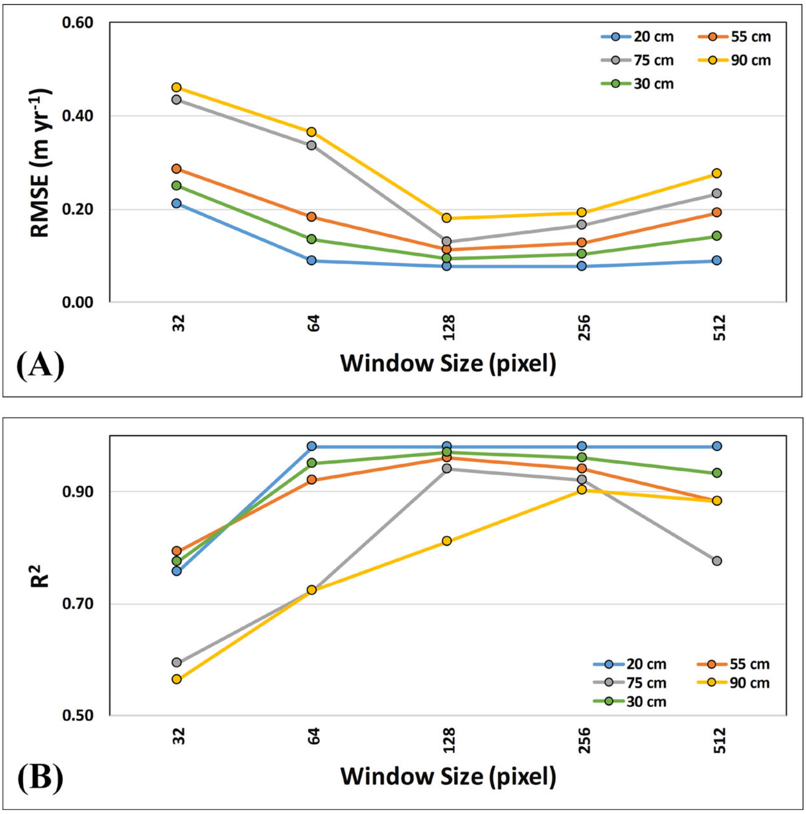

Figure 2. The behaviour of the image cross-correlation with varying window sizes: (A) RMSE errors and, (B) R^2 in comparison to manual digitisation points.

4. Results

4.1. The performance of window sizes

As it was shown in Figure 2, we evaluate the performance of 32, 64, 128, 256, and 512 window sizes over 20, 30, 55, 75, and 90 cm images, by comparison, the outputs of Cosi-Corr algorithms with manual digitisation points. Obtained results indicate that in 20 cm resolution images RMSE error was decreased from 32 to 64 window size but from 64 to 512 window size remains constant. Also, a similar pattern was found for the coefficient of determination. This process is not repeated for other images and the minimum RMSE error was found in 128 window size for all images. Also, R^2 values are often high for 128 window size in comparison to the other window sizes (except for the 90 cm image). Therefore, based on obtained results, as well as considering the maximum amount of glacier velocity, the initial and final window sizes are set to 128 and 32 for GSV measurement, respectively for all 19 different spatial resolution image sets.

4.2. Accuracy assessment using manual digitisation

To evaluate the performance of UAV images with different resolutions in GSV measurement, image cross-correlation outputs were compared with 110 manual GSV measurements. It should be noted that manual digitisation was performed on the original ortho-image with 10 cm resolution. Figure 3 shows scatter plots of the COSI-Corr outputs for

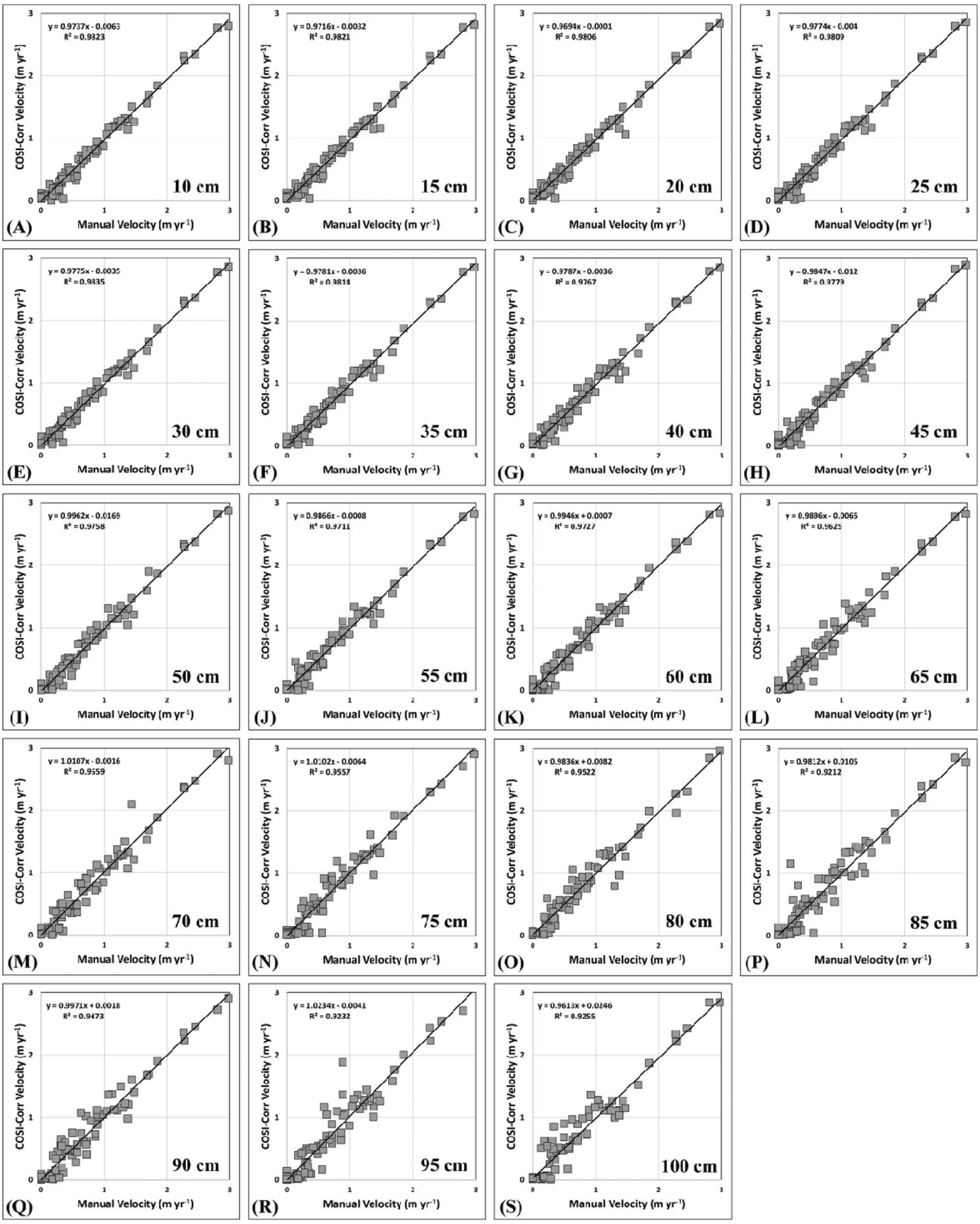

Figure 3. Manual GSV ($n = 110$) plotted against the COSI-Corr outputs for UAV imageries from 10 to 100 cm resolutions.

the 19 UAV products with resolutions from 10 to 100 cm against the manually digitised GSV. Also, the results of RMSE and coefficients of determination are summarised in Figure 4.

Based on the results obtained (Figure 3), the overall flow patterns for all generated GSVs are similar and the scatter plots are close to the 1:1 line with R^2 values range from the minimum of around 0.92 to the maximum of about 0.98. Mean velocity errors and

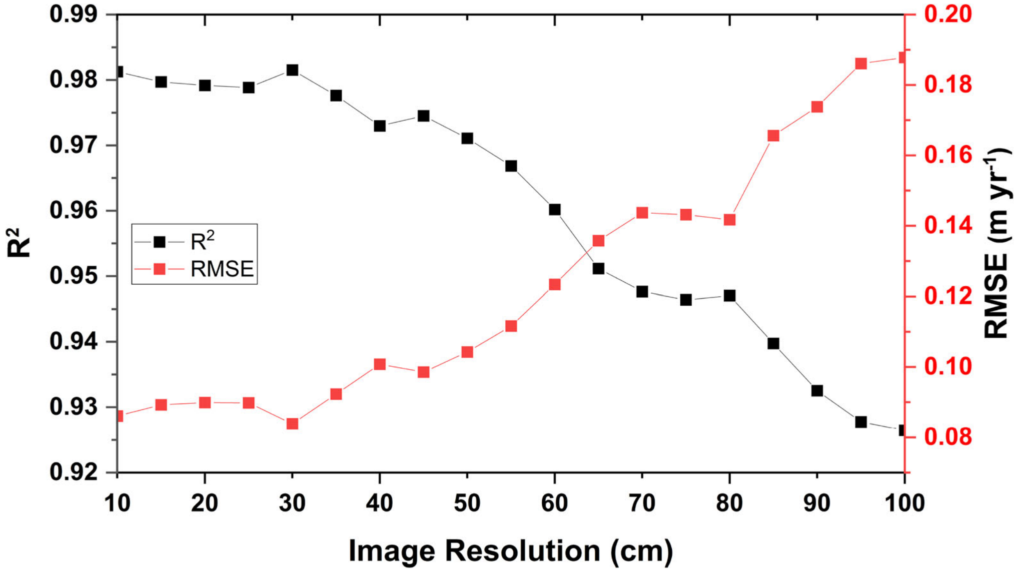

Figure 4. The behaviour of the image cross-correlation errors (RMSE and R^2) in comparison to manual digitisation points, with varying GSD in ortho-images.

the slopes of the fitted linear regression suggest a very slight and negligible underestimation of GSV by the COSI-Corr. Underestimation behaviour of frequency-based methods has been reported in areas with the presence of displacement gradient (e.g. Dematteis and Giordan 2021; Heid and Kääb 2012a). This underestimation occurs in areas where the features that move slower change less their texture.

Figure 4 summarised the behaviour of the GSV measurement errors with varying image resolution in orthophotos. According to the results, RMSE error increased towards the coarse images. While, the values of the coefficient of determination (R^2) gradually decreased towards the coarse images. The general trend of RMSE indicate that with the finer image resolutions, the GSV has also been calculated more accurately. Also, Coefficient of determination (R^2) was decreased as image resolutions decreased. Consequently, the highest R^2 between the measured GSV and manual digitisation was obtained in images with resolutions of 10–30 cm. In addition, RMSE error varies with the minimum value of about 0.083 m yr^{-1} in images with resolutions of 10 to 40 cm to the maximum value in 100 cm image (about 0.187 m yr^{-1}). Error values in 10–30 cm images are not significantly different and their accuracies are very similar to each other. While, from a 35 cm resolution and above, the accuracy of the obtained GSVs results is gradually reduced. Accordingly, based on obtained results, the optimal image resolution cannot be considered the finest resolution. Because, as shown in Figures 3 and 4, there is no noticeable differences between the 10 and 30 cm images in terms of error values and coefficients of determination and 30 cm image show the highest and lowest values of R^2 and RMSE, respectively in comparison to the finest image.

4.3. Accuracy assessment over off-glacier static areas

Figure 5 illustrate histograms of the GSV calculated by COSI-Corr over the stagnant non-glaciated area. Based on obtained results, as image resolution decreased, the histograms

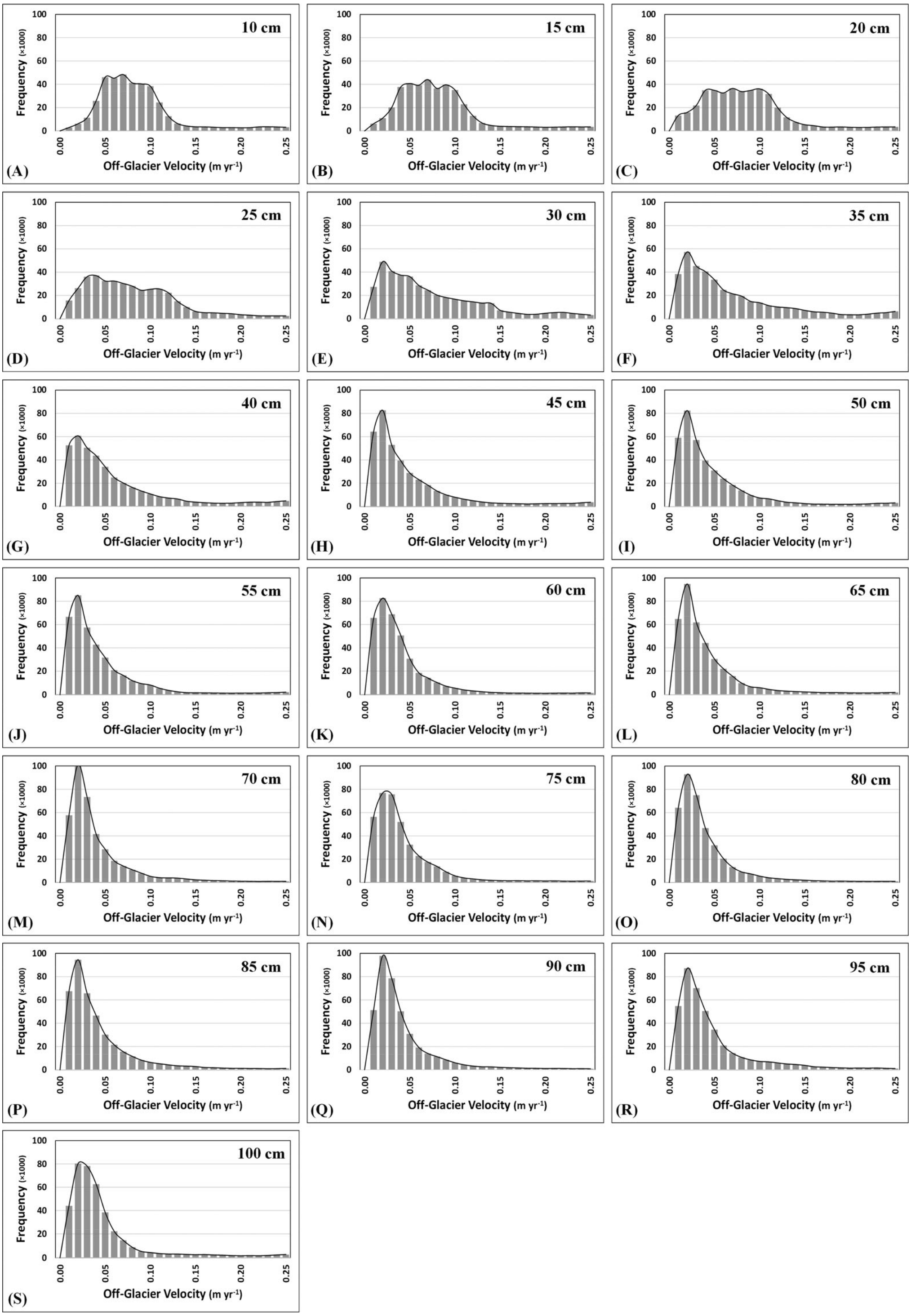

Figure 5. Histograms of velocities at non-dynamic off-glacier areas, as calculated by COSI-Corr for UAV images from a resolution of 10 to 100 cm.

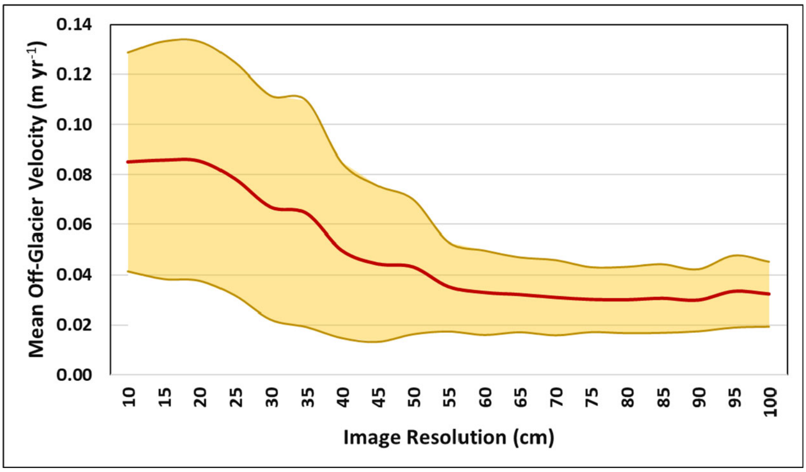

Figure 6. Mean off-glacier velocity deviations and associated standard deviations (yellow buffer), in all image resolutions.

are skewed to the left (close to zero) and the mean deviation of GSVs calculated using a cross-correlation algorithm have tended towards the expected zero value. The shape of histograms in 10–25 cm images shows a wide range of GSV deviations over the off-glacier area. These unusual distributions indicate a high standard deviation of the calculated GSV over the non-glaciated area in high-resolution images (<25 cm). While, from 30 cm image to the lower resolution images, all data sets follow the basic usual distribution curve. These results confirmed the practical absence of movement in 30 to 100 cm images.

The mean off-glacier velocity and associated standard deviations (orange buffer) are summarised in Figure 6. The maximum (0.085 m yr^{-1}) and minimum (0.032 m yr^{-1}) off-glacier velocity errors were found in 10 and 100 cm images, respectively. Obtaining the maximum values of off-glacier error over the off-glacier area on the 10 cm image is not so unexpected. Because, the finer resolution images capture very high detailed information of ground features (e.g. shadow, vegetation cover, and rockfalls), which would add several noises to UAV measurements. While, in coarse images, the noise of images is also reduced gradually. This noise reduction reduces the amount of uncertainties over the non-glaciated areas.

5. Discussion

5.1. Spatial analysis of results

Figure 7 shows the distribution of differences (%) between the velocity derived from COSI-Corr and manual digitisation points in all 19 UAV images with different resolutions. In the *Y*-axis of this plot, all 110 manually selected points are arranged from the minimum off-glacier values to the maximum values over the glacier surface. As shown in this figure, the minimum differences (the COSI-Corr result is divided into the manual digitisation point) are observed at points selected over the off-glacier area. In this static area, the differences vary from 0% to 15%. The main point about the off-glacier area is that the calculated velocities are underestimated by the COSI-Corr method, and no one has been overestimated. As discussed in Section 4.1, the underestimation behaviour of frequency-based methods has been reported by several researchers. This underestimation

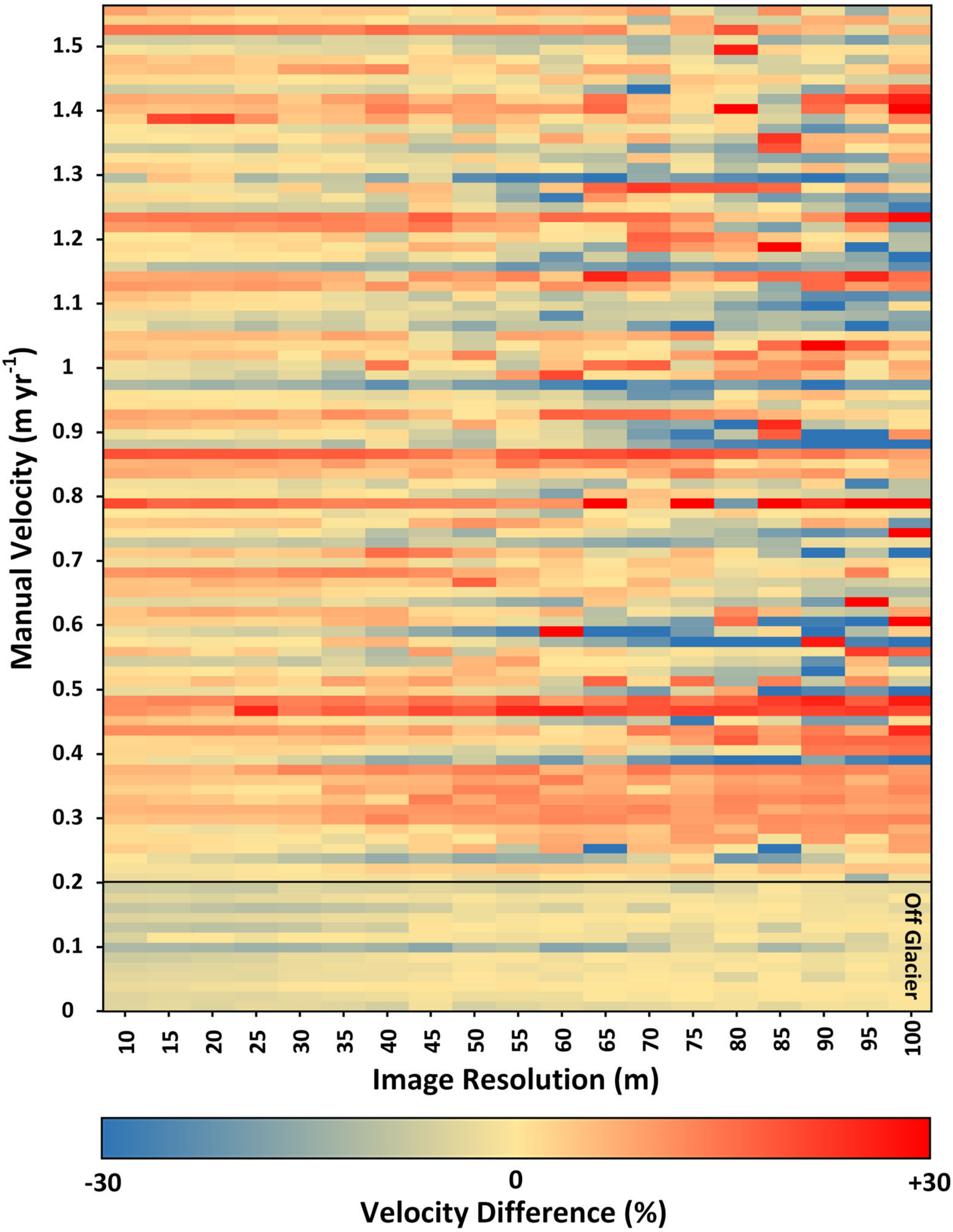

Figure 7. Relation between velocity and velocity differences (difference between the velocity values derived from COSI-Corr and the velocity values derived from the manual digitisation) in different spatial resolution UAV images.

varies between 5% and 15% in images with resolutions from 10 to 40 cm. While, in images coarser than the 40 cm, the differences are actually reduced. Therefore, over the off-glacier area, as the image resolution increased, the differences of the COSI-Corr method has been gradually reduced.

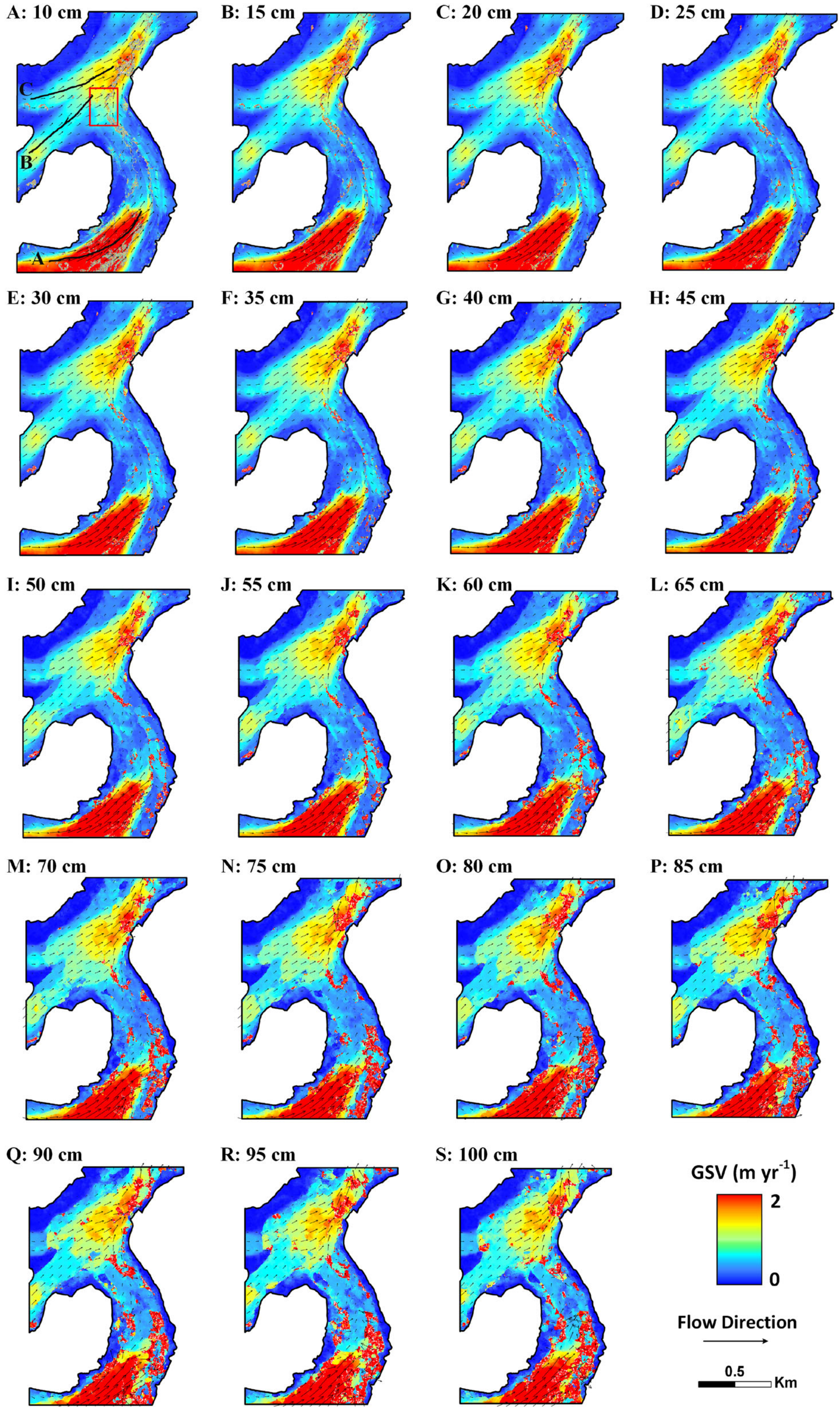

Figure 8. GSV results were obtained from frequency cross-correlation of UAV images with variable resolution from 10 to 100 cm.

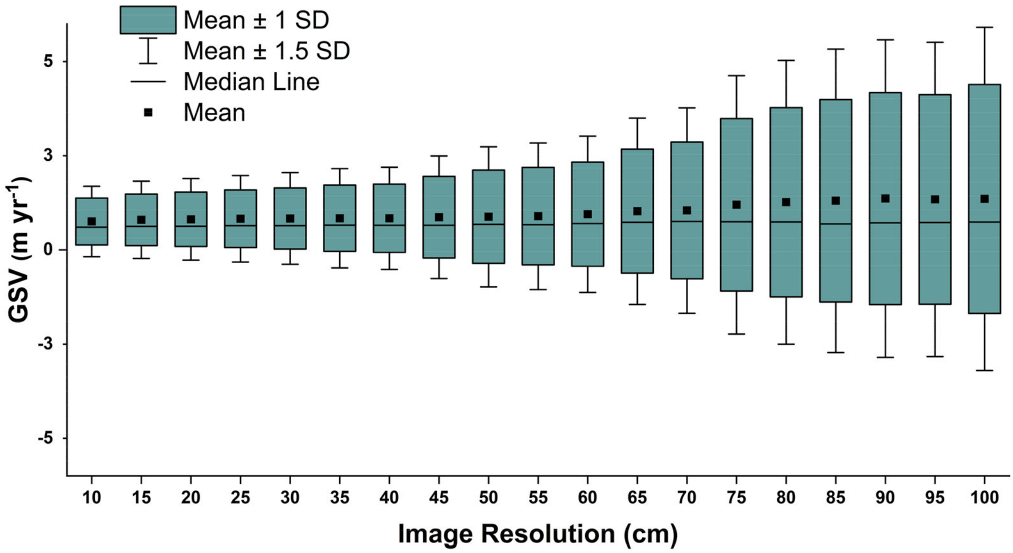

Figure 9. Boxplot and spread of the GSV at different spatial resolution from 10 to 100 cm at the 100 cm spatial domain.

Contrarily to the points over the off-glacier area, points over the surface of the glacier show quite a different behaviour. At these points, in coarser images, the differences have also increased. Differences increased more clearly from 45 to 100 cm image.

As can be seen in Figure 7, no clear overestimation or underestimation of GSV can be found in images with resolutions lower than 45 cm. But in images with resolutions greater than 45 cm, the predominant pattern is the overestimation of velocity (about +3%). Differences of all points in each image show that there is no clear systematic error in COSI-Corr outputs. This indicates that the differences are homogeneously distributed throughout the glacier surface.

The resulting GSV maps are shown in Figure 8. The vectors plotted on the maps represent the GSV direction in 5 m resampled image resolution. As illustrated in this figure, the general GSV magnitude and direction are similar for all data sets. A noticeable difference in coarser images, irregularly distributed noise (pixels with SNR lower than 0.90) is abundant, and the 10 to 40 cm images show the least noise. Such noises are often found around ice cliffs and supraglacial ponds. The higher noise abundance in coarser images is possible because as the pixel size increase, the small debris-cover and boulders are not detectable on images and this is resulting in mismatches of the correlator. The results indicate that the GSV varies from 2 m yr^{-1} in high elevated regions to about zero in glacier borders.

For comparing the mean GSV and the distribution of obtained results by all images, first the outliers are removed from the images (pixels with GSV greater than 5 m yr^{-1} was discarded). Because in all obtained GSV maps, different outliers of GSV can be found and these values can make a significant bias in mean GSV results. The existence of outliers is more of an issue in coarse images (as it was shown in Figures 8 and 11). Figure 9 shows the boxplot of GSVs with associated mean, median and mean ± 1 SD and 1.5 SD (standard deviation) for all resolution images. As spatial domain of all images is different, the 100 cm minimum spatial domain was used to calculate the comparable results. Based on the obtained results, while the median GSV for all images are equal, the mean and SD are different. 10 cm image shows the minimum value of mean GSV (about 0.75 m yr^{-1})

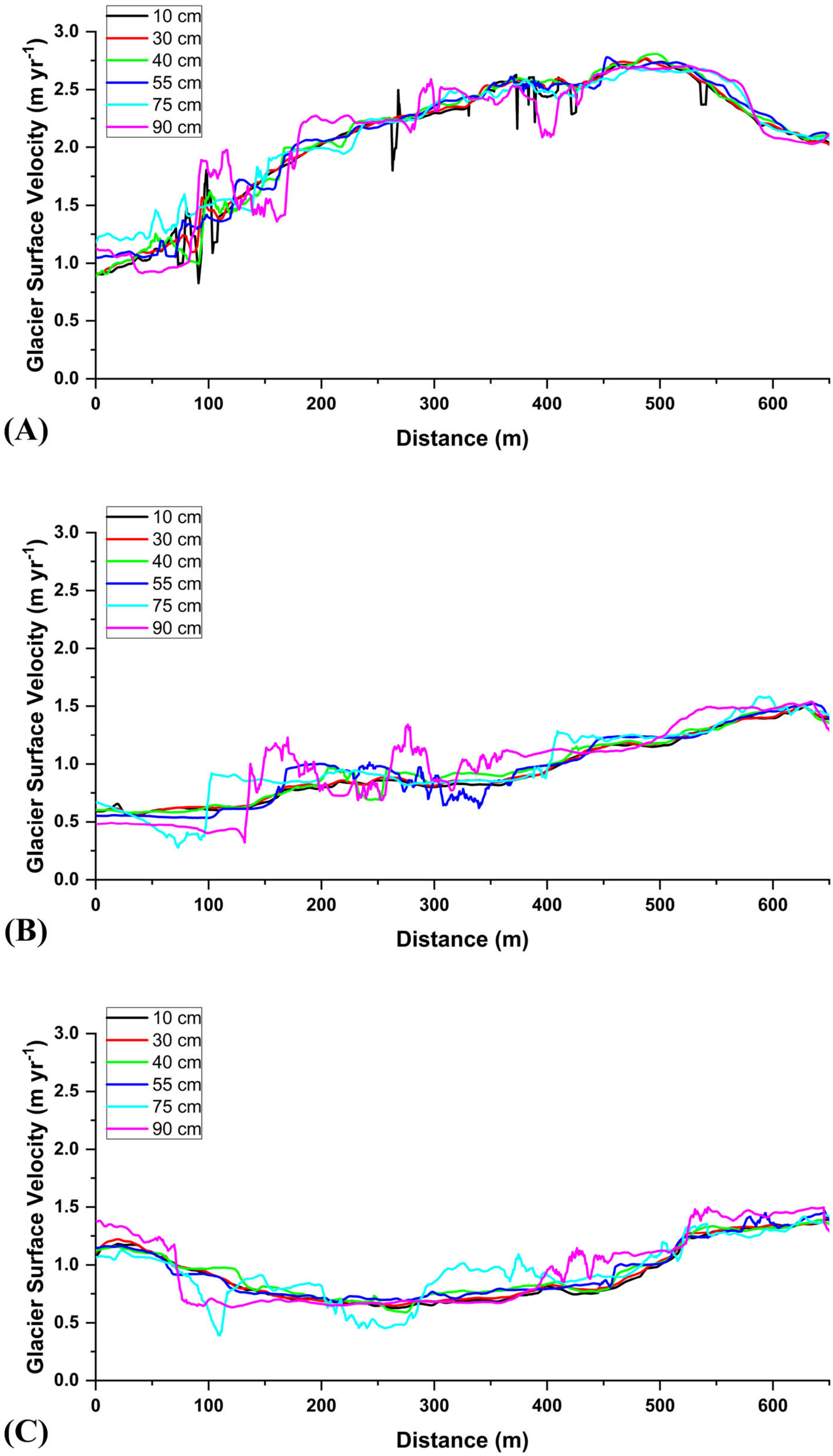

Figure 10. Glacier surface velocity (m yr^{-1}) profiles for images with resolutions equal to 10, 30, 40, 55, 75, and 90 cm.

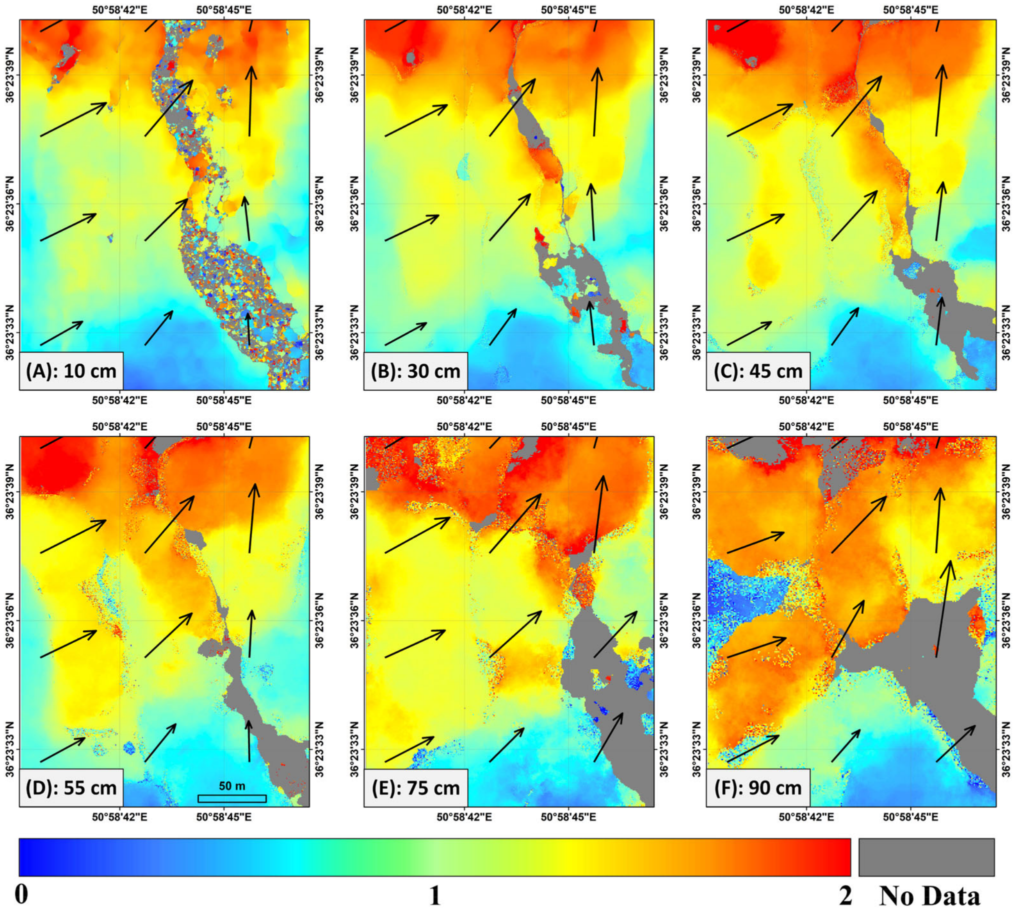

Figure 11. Examples of glacier surface velocity (m yr^{-1}) result at different image resolutions. No data values (SNR < 0.9) were shown as grey colour. The corresponding area was indicated in Figure 8(A) as a red box.

and it was towards the coarser images. The mean GSV in the 100 cm image reached about 1.35 m yr^{-1} which is 1.8 times greater than the 10 cm image. Indeed, in coarse images, the mean GSV of glacier was increased but the mean GSV calculated in the 10–60 cm resolution images are very close and no specific variation can be observed. Accordingly, the GSV standard deviations have increased from the fine resolution images towards the coarse images. The maximum standard deviation was found in 100 cm image while, the boxes for 10–35 cm are on a similar level and standard deviations have not varied significantly. Such high standard deviation in coarse resolution images leads to the high level of overestimation in mean GSV, while the median GSV was not affected.

In Figure 10, three longitudinal GSV transect for images with resolutions equal to 10, 30, 40, 55, 75, and 90 cm are shown as an example. The general process of all images is quite similar in estimating GSV, but they differ greatly in detail. The coarser images were found to measure the GSV with highly heterogeneous, while the lowest heterogeneity of GSVs was found in fine images.

Figure 11 shows examples of GSV results at different image resolutions. In this image, low SNR areas were discarded and shown as no data (grey colour). As illustrated in this figure, among the different resolution images, 90 cm image has the largest proportion of the low SNR values (about 16.8%), while smaller low-quality areas are much lower at fine resolution images. The proportion of low SNR area in this subset region was about 7.62%, 4.95%, 5.56%, 6.02%, 10.51%, and 16.8% in 10, 30, 45, 55, 75, and 90 cm images, respectively.

At finer images (especially in 30 and 45 cm images), the values of GSVs are more homogenous and smoother. While, at coarse images, several no data and Inconsistency in GSV can be found and the GSV results are more heterogeneous.

It is worth to note that the results obtained in the present case study cannot represent of every site and therefore our results cannot extend to all glaciers. While in the present study we just want to show the impact of UAV image resolution on the accuracy of GSV measurement for small glaciers located in arid and semi-arid environments where flow velocities are not exceeding a few metres per year. Such glaciers are abundant in Iran and the high mountain of Asia. Regardless of the size and ice volume of such glaciers, these glaciers are very valuable and important as climate change sensors.

6. Conclusions

The use of UAV platforms allows calculation of very high-resolution glacier GSV, something not possible with medium to low resolution space-borne satellite platforms. Our approach yields insights into the performance of different UAV resolution images in GSV measurement and improves our understanding of the optimal image resolution for small debris-covered GSV monitoring.

Based on accuracy assessment using manual digitisation points and off-glacier velocity evaluation, we can conclude that the best result of GSV was not obtained using the highest resolution image. While, the quality of the results of the images between 10 and 30 cm is substantially the same Results revealed that 30 cm GSD image shows the minimum uncertainty over the off-glacier area. In addition, the highest linear correlation coefficient between the measured GSV and manual digitisation was obtained in a 30 cm resolution image. Also, RMSE, and R^2 were obtained around 0.083 m yr^{-1}, and 0.98, respectively in a 30 cm GSD image. In conclusion, if the UAV images are taken with very high resolution, there is no need to use the highest resolution to measure the velocity of glaciers. Because by using the highest resolution image, only the processing time and the volume of unnecessary information increased, while the accuracy of the results is not in the best possible condition. Therefore, it is recommended that original UAV images be resampled to about 30 cm to obtain the optimal results with the highest possible accuracy. It is worth to note that this conclusion is just based on the spatial resolution of UAV images. However, many other parameters such as the flow velocity, glacier surface pattern, camera specifications, geocoding uncertainty can also affect the selection of the best image.

Our findings can provide instruction when deciding which image resolution to use for GSV measurement in similar study areas. The main conclusions are as follows:

1. The results show that using too fine resolution images will lead to computational redundancy and a 30 cm grid cell size has a better performance in GSV estimation rather than higher resolution images. In addition, GSV measurements become worse with coarser resolution (especially between 45 and 100 cm);
2. Very high-resolution images (better than 25 cm) should be used for studies where very high accuracy of the results is required and the glacier velocity is not noticeable;
3. Images with a coarse resolution (greater than 50 cm) should be used where a general and non-detailed outlook of glacier velocity is required, but the quality and quantity of GSV results are not as crucial as in detailed studies. Processing such images

requires less time and hardware, and the obtained GSV results are still commensurable to the finer resolution images.

4. Using a 30 cm image to measure the glacier surface velocity compared to the original 10 cm image results in an approximately 8.3 times reduction in processing time. In addition, as window size increased, the processing time increased quadratically. Consequently, selecting optimal image resolution and window size for GSV measurement can significantly reduce processing time.

Acknowledgements

The author deeply appreciates the support received from the Water Research Institute for providing data and facilities.

Disclosure statement

No potential conflict of interest was reported by the author.

ORCID

Neamat Karimi http://orcid.org/0000-0002-7896-4390

References

Ahn Y, Box JE. 2010. Instruments and methods glacier velocities from time-lapse photos: technique development and first results from the Extreme Ice Survey (EIS) in Greenland. J Glaciol. 56(198):723–734.

Bash EA, Moorman BJ, Gunther A. 2018. Detecting short-term surface melt on an Arctic glacier using UAV surveys. Remote Sens. 10(10):1547.

Brun F, Wagnon P, Berthier E, Shea JM, Immerzeel WW, Kraaijenbrink PDA, Vincent C, Reverchon C, Shrestha D, Arnaud Y. 2018. Ice cliff contribution to the tongue-wide ablation of Changri Nup Glacier, Nepal, central Himalaya. Cryosphere. 12(11):3439–3457.

Dehecq A, Gourmelen N, Gardner AS, Brun F, Goldberg D, Nienow PW, Berthier E, Vincent C, Wagnon P, Trouvé E. 2019. Twenty-first century glacier slowdown driven by mass loss in High Mountain Asia. Nature Geosci. 12(1):22–27.

Dehecq A, Gourmelen N, Trouve E. 2015. Deriving large-scale glacier velocities from a complete satellite archive: Application to the Pamir-Karakoram-Himalaya. Remote Sens Environ. 162:55–66.

Dematteis N, Giordan D. 2021. Comparison of digital image correlation methods and the impact of noise in geoscience applications. Remote Sens. 13(2):327.

Evans AN. 2000. Glacier surface motion computation from digital image séquences. IEEE Trans Geosci Remote Sens. 38(2):1064–1072.

Farajzadeh M, Karimi N. 2014. Evidence for accelerating glacier ice loss in the Takht'e Solaiman Mountains of Iran from 1955 to 2010. J Mt Sci. 11(1):215–235.

Fey C, Krainer K. 2020. Analyses of UAV and GNSS based flow velocity variations of the rock glacier Lazaun (Ötztal Alps, South Tyrol, Italy). Geomorphology. 365:107261.

Fugazza D, Senese A, Azzoni RS, Smiraglia C, Cernuschi M, Severi D, Diolaiuti GA. 2015. High-resolution mapping of glacier surface features. The uav survey of the forni glacier (Stelvio National Park, Italy). Geografia Fisica e Dinamica Quaternaria. 38(1):25–33.

Gentili R, Baroni C, Panigada C, Rossini M, Tagliabue G, Armiraglio S, Citterio S, Carton A, Salvatore MC. 2020. Glacier shrinkage and slope processes create habitat at high elevation and microrefugia across treeline for Alpine plants during warm stages. Catena. 193(May 2019):104626.

Heid T, Kääb A. 2012a. Evaluation of existing image matching methods for deriving glacier surface displacements globally from optical satellite imagery. Remote Sens Environ. 118:339–355.

Heid T, Kääb A. 2012b. Evaluation of existing image matching methods for deriving glacier surface displacements globally from optical satellite imagery. Remote Sens Environ. 118:339–355.

Immerzeel WW, Kraaijenbrink PDA, Shea JM, Shrestha AB, Pellicciotti F, Bierkens MFP, De Jong SM. 2014. High-resolution monitoring of Himalayan glacier dynamics using unmanned aerial vehicles. Remote Sens Environ. 150:93–103.

Intergovernmental Panel on Climate Change, editor. 2014. Observations: cryosphere. In Climate change 2013 – the Physical Science basis: Working Group I contribution to the Fifth Assessment Report of the Intergovernmental Panel on Climate Change. Cambridge: Cambridge University Press; p. 317–382.

Jouvet G, Weidmann Y, Kneib M, Detert M, Seguinot J, Sakakibara D, Sugiyama S. 2018. Short-lived ice speed-up and plume water flow captured by a VTOL UAV give insights into subglacial hydrological system of Bowdoin Glacier. Remote Sens Environ. 217(August):389–399.

Jouvet G, Weidmann Y, van Dongen E, Lüthi MP, Vieli A, Ryan JC. 2019. High-endurance UAV for monitoring calving glaciers: application to the Inglefield Bredning and Eqip Sermia, Greenland. Front Earth Sci. 7:206.

Kääb A, Leinss S, Gilbert A, Bühler Y, Gascoin S, Evans SG, Bartelt P, Berthier E, Brun F, Chao WA, et al. 2018. Massive collapse of two glaciers in western Tibet in 2016 after surge-like instability. Nature Geosci. 11(2):114–120.

Karimi N, Farajzadeh M, Moridnejad A, Namdari S. 2014. Evidence for mountain glacier changes in semi-arid environments based on remote sensing data. J Indian Soc Remote Sens. 42(4):801–815.

Karimi N, Farokhnia A, Sheshangosht S, Bahreinimotlagh M. 2021a. Using UAV and satellite image data for analyzing the elevation change of debris-covered glaciers and its associated driving factors. Environ Earth Sci. 80(17):577.

Karimi N, Sheshangosht S, Farokhnia A. 2022. Determining the spatio-temporal variability of glacier surface velocity using high-resolution satellite images and UAV data: Alamkuh glacier, Iran. Remote Sens Lett. 13(2):138–150.

Karimi N, Sheshangosht S, Roozbahani R. 2021b. High-resolution monitoring of debris-covered glacier mass budget and flow velocity using repeated UAV photogrammetry in Iran. Geomorphology. 389: 107855.

Kaufmann V. & Ladstädter, R. 2008. Application of terrestrial photogrammetry for glacier monitoring in Alpine environments. In: Proceedings of the 21st Congress of ISPRS; 37; Part B. p. 813–818. http://geo-imaging.tugraz.at/viktor.kaufmann/ISPRS2008Beijing_Kaufmann.pdf.

Kaufmann V. 2012. The evolution of rock glacier monitoring using terrestrial photogrammetry: the example of Äusseres Hochebenkar rock glacier (Austria). Austrian J Earth Sci. 105(2):63–77.

Kraaijenbrink P, Meijer SW, Shea JM, Pellicciotti F, De Jong SM, Immerzeel WW. 2016. Seasonal surface velocities of a Himalayan glacier derived by automated correlation of unmanned aerial vehicle imagery. Ann Glaciol. 57(71):103–113.

Kraaijenbrink PDA, Shea JM, Litt M, Steiner JF, Treichler D, Koch I, Immerzeel WW. 2018. Mapping surface temperatures on a debris-covered glacier with an unmanned aerial vehicle. Front Earth Sci. 6(May):1–19.

Kraaijenbrink PDA, Shea JM, Pellicciotti F, Jong S. M d, Immerzeel WW. 2016. Object-based analysis of unmanned aerial vehicle imagery to map and characterise surface features on a debris-covered glacier. Remote Sens Environ. 186:581–595.

Leprince S, Ayoub F, Klinger Y, Avouac JP. 2007. Co-registration of optically sensed images and correlation (COSI-Corr): an operational methodology for ground deformation measurements. In: International Geoscience and Remote Sensing Symposium (IGARSS). p. 1943–1946.

Lo Vecchio A, Lenzano MG, Durand M, Lannutti E, Bruce R, Lenzano L. 2018. Estimation of surface flow speed and ice surface temperature from optical satellite imagery at Viedma glacier, Argentina. Global Planet Change. 169(May 2017):202–213.

Maas H-G, Dietrich R, Schwalbe E, Bäßler M, Westfeld P. 2006. Analysis of the motion behaviour of Jakobshavn Isbrae glacier in Greenland by monocular image sequence analysis. Int. Arch. Photogramm. 36(May 2014):179–183.

Millan R, Mouginot J, Rabatel A, Jeong S, Cusicanqui D, Derkacheva A, Chekki M. 2019. Mapping surface flow velocity of glaciers at regional scale using a multiple sensors approach. Remote Sens. 11(21): 2498.

Paul F, Bolch T, Kääb A, Nagler T, Nuth C, Scharrer K, Shepherd A, Strozzi T, Ticconi F, Bhambri R, et al. 2015. The glaciers climate change initiative: Methods for creating glacier area, elevation change and velocity products. Remote Sens Environ. 162:408–426.

Rai SP, Singh D, Jacob N, Rawat YS, Arora M. BhishmKumar 2019. Identifying contribution of snowmelt and glacier melt to the Bhagirathi River (Upper Ganga) near snout of the Gangotri Glacier using environmental isotopes. Catena. 173:339–351.

Ramsankaran R, Navinkumar PJ, Dashora A, Kulkarni AV. 2021. UAV-based survey of glaciers in Himalayas: challenges and recommendations. J Indian Soc Remote Sens. 49(5):1171–1187.
Redpath TAN, Sirguey P, Fitzsimons SJ, Kääb A. 2013. Accuracy assessment for mapping glacier flow velocity and detecting flow dynamics from ASTER satellite imagery: Tasman glacier, New Zealand. Remote Sens Environ. 133:90–101.
Robson BA, Macdonell S, Ayala Á, Bolch T, Nielsen PR, Vivero S. 2021. Glacier and Rock Glacier changes since the 1950s in the La Laguna catchment, Chile. Cryosphere. 1–34.
Scherler D, Leprince S, Strecker MR. 2008. Glacier-surface velocities in alpine terrain from optical satellite imagery-accuracy improvement and quality assessment. Remote Sens Environ. 112(10):3806–3819.
Scherler D, Strecker MR. 2012. Large surface velocity fluctuations of Biafo glacier, central Karakoram, at high spatial and temporal resolution from optical satellite images. J Glaciol. 58(209):569–580.
Shukla A, Garg PK. 2020. Spatio-temporal trends in the surface ice velocities of the central Himalayan glaciers, India. Global Planet Change. 190(April):103187.
Śledź S, Ewertowski MW, Piekarczyk J. 2021. Applications of unmanned aerial vehicle (UAV) surveys and structure from motion photogrammetry in glacial and periglacial geomorphology. Geomorphology. 378:107620.
Storni E, Hugentobler M, Manconi A, Loew S. 2020. Monitoring and analysis of active rockslide-glacier interactions (Moosfluh, Switzerland). Geomorphology. 371:107414.
Sugiyama S, Fukui K, Fujita K, Tone K, Yamaguchi S. 2013. Changes in ice thickness and flow velocity of Yala Glacier, Langtang Himal, Nepal, from 1982 to 2009. Ann Glaciol. 54(64):157–162.
Tanarro LM, Palacios D, Andrés N, Fernández-Fernández JM, Zamorano JJ, Saemundsson Þ, Brynjólfsson S. 2019. Unchanged surface morphology in debris-covered glaciers and rock glaciers in Tröllaskagi peninsula (northern Iceland). Sci Total Environ. 648:218–235.
Vincent C, Wagnon P, Shea JM, Immerzeel WW, Kraaijenbrink P, Shrestha D, Soruco A, Arnaud Y, Brun F, Berthier E, et al. 2016. Reduced melt on debris-covered glaciers: investigations from Changri Nup glacier, Nepal. Cryosphere. 10(4):1845–1858.
Vivero S, Lambiel C. 2019. Monitoring the crisis of a rock glacier with repeated UAV surveys. Geogr Helv. 74(1):59–69.
Watson CS, Kargel JS, Shugar DH, Haritashya UK, Schiassi E, Furfaro R. 2020. Mass loss from calving in Himalayan proglacial lakes. Front Earth Sci. 7(January):1–19.
Wigmore O, Mark B. 2017. Monitoring tropical debris-covered glacier dynamics from high-resolution unmanned aerial vehicle photogrammetry, Cordillera Blanca, Peru. Cryosphere. 11(6):2463–2480.